Structural Role of the Proline Residues of the β-Hinge Region of p13^{suc1} As Revealed by Site-Directed Mutagenesis and Fluorescence Studies†

Federica Simeoni, Lanfranco Masotti, and Paolo Neyroz*

Dipartimento di Biochimica "G. Moruzzi", Università degli Studi di Bologna, Via San Donato, 19/2, I-40127 Bologna, Italy

Received December 12, 2000; Revised Manuscript Received April 12, 2001

ABSTRACT: Site-directed mutagenesis, gel filtration, and fluorescence spectroscopy approaches were used to study the molecular hinge mechanism involved in the β-strand-exchanged dimer formation of the cyclin-dependent protein kinase regulatory subunit p13^{suc1} from *Schizosaccharomyces pombe.* Single and double mutants of residues Pro-90 and Pro-92 (P90V, P92V, and P90V/P92V) were prepared and assayed. Substitution of Pro-90 prevented dimer formation by arm exchange. However, single point mutations did not affect the two-state unfolding transition of wild-type p13^{suc1} at equilibrium (i.e., wild type, $\Delta G^{\circ}_{0,un} = 7.38 \pm 0.35$ kcal mol^{-1}, vs P90V, $\Delta G^{\circ}_{0,un} = 6.71 \pm 0.18$ kcal mol^{-1}). On the contrary, the double mutant unfolded with a complex transition, and the reaction was best described by a three-state model (N ⇆ I ⇆ U). Resolution of the state-dependent (native vs denatured) intrinsic fluorescence decay amplitudes of p13^{suc1} showed that with P90V/P92V these parameters were affected at [GuHCl] significantly less than with wild-type and single mutant proteins. Moreover, with the latter products, fluorescence quenching measurements at 1 M GuHCl revealed linear Stern−Volmer plots with quenching constants typical of tryptophan residues located in a native environment (1.6 M^{-1} < K_{SV} < 2.3 M^{-1}). Dissimilarly, with P90V/P92V a significant deviation from linearity of the Stern−Volmer plot was obtained. Nonlinear least-squares analysis of these data resolved the significant contribution of highly solvent-accessible emitting species (K_{SV} = 26 M^{-1}) consistent with large exposure of the tryptophan residues. These results are compatible with the existence of an intermediate unfolding state of the double mutation product. Thus, while single residue substitution studies give support to the primary role of Pro-90 in the p13^{suc1} dimer formation by domain swapping, double residue substitution studies indicate the important role of the conserved repeat, Pro-x-Pro, for the proper β-strand spatial organization and stability.

The formation of cyclin-dependent kinase (CDK) complexes and their sequential activation are major events in controlling the cell cycle progression (*1*). The phosphorylation of conserved threonine residues (Thr-160 in CDK2 and Thr-161 in Cdc2) by the CDK-activating complex (CAK) is required for their activation, and full biological activity is achieved by the assembly of the catalytic subunit with cyclins. In turn, CDK inactivation is maintained by inhibitor proteins (CKI) (*2*) and by inhibitory phosphorylation of conserved residues near the amino terminus (Thr-14 and Tyr-15 in CDK2 and Cdc2) catalyzed by Wee1 and Myt1 (*3*−*5*). In addition, because of the positive regulatory role of cyclins, their periodic degradation marks the end of a specific CDK complex activity.

The biochemical and the cell biology dissections of the crucial mechanisms in the control of the cell division cycle have led to the definition of check points and have shown how protein−protein interactions and posttranslational events represent the actual molecular triggers for proper progression throughout DNA replication and cell division. In this respect, the resolution of the crystal structure of the isolated elements (i.e., CDK2 and cyclin A) (*6*, *7*) and their complexes (*8*−*10*) has provided relevant information for understanding the structural basis and the conformational changes involved in the modulation of CDK activity. In addition to the best characterized regulatory effectors of the CDK biological activity, some essential functions are performed by the CDK1- and CDK2-binding protein family (CKS, cyclin-dependent kinase subunit): a group of small proteins (9−18 kDa), with highly conserved sequences (50−80% sequence identity) and a high functional homology (*11*), which act in higher eukaryote cell cycle control. The prototype members of this class were isolated from *Saccharomyces cerevisiae* (Cks1, Cdc28 kinase subunit) (*12*) and from *Schizosaccharomyces pombe* (p13^{suc1}, suppressor of cell cycle) (*13*). Homologues have been found in all animal eukaryotes and also in plants (*14*).

p13^{suc1}, originally identified as extragenic suppressor of certain CDC2 temperature-sensitive mutations (*13*), was found associated with the major cell cycle regulator, p34^{cdc2}, and its binding to this cyclin-dependent kinase has been widely used in many biological assays in vitro (*15*). In association with CDK1/CDK2 kinases, p13^{suc1}'s biological function is particularly essential in the G0/M phase (*11*), where it also affects Cdc25 phosphatase activity and

† This work was supported by Italian Research National Council (C.N.R.) Grant 98.00483.CT04 to P.N. and a MURST-PRIN grant to L.M. A preliminary account of this work was presented at the Sixth International Conference on Methods and Applications of Fluorescence Spectroscopy, held in Paris Sept 12−15, 1999.

* To whom correspondence should be addressed: e-mail, neyroz@biocfarm.unibo.it; phone, ++39-51-253528; fax, ++39-51-242978.

10.1021/bi002812d CCC: $20.00
Published on Web 06/13/2001

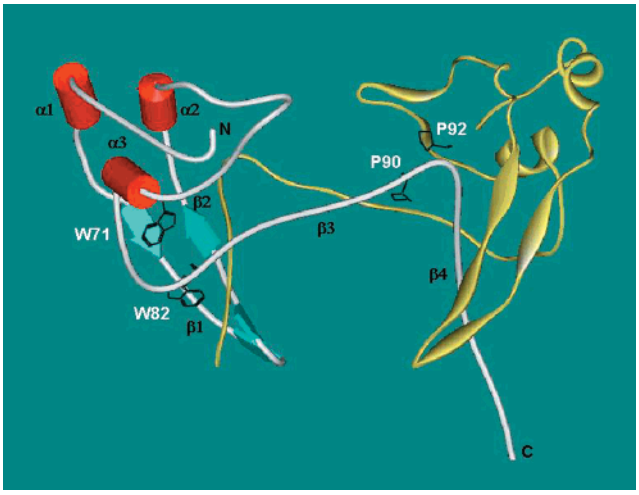

FIGURE 1: Diagram of the CKS β-strand-exchanged dimer assembly. The diagram was prepared from the crystallographic structure data file 1sce.pdb (*23*) using the program WebLabViewerPro (Molecular Simulation Inc.). In the chain represented on the left as schematic secondary type are indicated the secondary structure assignments. The β-hinge proline residues (single-letter amino acid code) of this chain are outlined together with the tryptophan residues. The partner monomer subunit is represented on the right as solid ribbon type.

abrogates kinase activation by Thr-14/Tyr-15 dephosphorylation (*16*). In fact, p13^{suc1} inhibits the entry into mitosis in *Xenopus* extracts (*17*) as well as meiotic reinitiation in mammalian oocytes (*18*). In consistent agreement with these findings, p9, the homologous CKS in *Xenopus*, has been found recently to stimulate the regulatory phosphorylation of Cdcd25, Myt1 and Wee1 that are carried out by the Cdc2/cyclin B complex (*19*).

Finally, both p9 (*20*) and p13^{suc1} (*21*, *22*) have been suggested to facilitate substrate recognition in the ubiquitin-mediated proteolysis of cyclin B by the cyclosome (the anaphase-promoting complex, APC), thus acting in the late phases of mitosis.

The crystal structure of different CKS have been solved, including p13^{suc1} (*23*−*25*) and the human homologues CksHs2 (*26*) and CksHs1 (*27*). Intriguingly, in all of these studies a peculiar oligomeric assembly has been revealed. In particular, with p13^{suc1} and CksHs1 an unusual β-strand-exchanged dimer form has been found (Figure 1). In these dimeric structures, β-strand 4 of each subunit is provided by the partner monomer subunit. This arrangement is reached with loss of a β-turn in a crucial hinge region of CKS, and the involved β-strand changes its spatial configuration from folded (inserted between β-strands 3 and 2), in the monomer, to extended, in the dimer. This transition has been recently referred in a review on proline-dependent oligomerization (*28*) to a domain swapping mechanism (*29*).

The exchanging β-hinge comprises the residues H^{88}xPEPH^{93} (single-letter amino acid code) that are conserved across all members of the CKS family. Site-directed mutagenesis analyses of CKS single mutants have been performed in two independent studies by substitution of Glu-63 of the human CksHs2 (*30*) and by substitution of the proline residues Pro-90 and Pro-92 of p13^{suc1} (*31*), respectively. Analyses on the human complex, CDK2−CksHs1, predict that important contacts between some crucial residues of CKSs (i.e., His-88, His-93, and Glu-91 of p13^{suc1}) and the CDK2 surface are precluded when the β-hinge is in the extended conformation (*27*). Indeed, it was found that replacing Glu-63 with glutamine modifies the CKD2 binding property of the CKS but does not impair its ability to form the dimer. On the other hand, replacement of the hinge residue Pro-90 with alanine appeared to prevent p13^{suc1} arm-exchanged subunit association.

More recently in blind studies, a complete protein engineering evaluation (*32*) and molecular dynamic simulations (*33*) on the folding pathway of p13^{suc1} provided evidence for a nucleation−condensation mechanism in which β-strand 4 forms an integral part of the folding nucleus. According to this view, separation in monomer and dimer forms represents an early event *via* unfolded states, and it has been emphasized (*32*; V. Daggett personal communication) how some aspects of these hypotheses could be remarkably consistent with previous experimental observations on the monomer−dimer equilibrium (*34*) and partial temperature stability (*35*) of p13^{suc1}.

In the present paper we have further probed the relevance of sequence/structure relationships of the β-hinge region on the overall stability and oligomerization properties of p13^{suc1}. Valine has been used to replace residues Pro-90 and Pro-92, and the single substitution products (P90V and P92V) have been analyzed by gel filtration chromatography and fluorescence methods. In addition, a double proline substitution (P90V/P92V) was inserted to test the role of the sequence Pro-x-Pro that has been proposed to represent a conserved motif among arm-exchanged proteins (i.e., SV40 and CKS) (*28*). The comparison of the data obtained with single and double mutation products is presented. p13^{suc1} contains two tryptophan residues (Trp-71 and Trp-82) located in the α-helix 3 and β-strand 3 regions, respectively, and their intrinsic fluorescence properties have been previously characterized under native and denaturing conditions (*35*). Here, the information provided by equilibrium denaturation studies has been examined at the steady-state as well as resolved in the nanosecond time domain. Finally, fluorescence quenching measurements performed in the presence of denaturant have been used to unravel the existence of protein species with distinct solvent accessibility.

On one hand, single mutant studies support the crucial role of residue Pro-90 on CKS dimerization by arm exchange; on the other hand, the double mutant studies reveal that both of the β-hinge prolines are required for the proper organization and stability of the CKS monomer β-strand cluster.

EXPERIMENTAL PROCEDURES

Materials. Guanidine hydrochloride (GuHCl),[1] melatonin, and the buffer salts were from Sigma-Aldrich Co. (St. Louis, MO) for molecular biology and electrophoresis reagent grade, respectively. T4 DNA ligase and *Nde*I and *Eco*RI restriction enzymes were from Takara Biomedicals (Japan). Sepharose CL6B and Sephacryl S-100HR were obtained from Amersham-Pharmacia Biotech AB (Uppsala, Sweden).

p13^{suc1} Protein Expression and Purification. p13^{suc1} was expressed and purified from *Escherichia coli* [BL21(DE3)]-

[1] Abbreviations: COM, center of mass; DAS, decay-associated spectra; FWHM, full width at half-maximum; GuHCl, guanidine hydrocloride.

pLysS cells. The *SUC1*-containing plasmids pTZ19R (mutation vector) and pRK172 (expression vector) were a kind gift from Dr. Jane Endicott (Laboratory of Molecular Biophysics, Oxford University, Oxford, U.K.). Bacterial growth and purification were carried out following the original procedure of Brizuela et al. (*15*) with minor modifications (*35*). The same procedures were used for the wild-type and the mutant proteins. The purified proteins were concentrated to 0.5−2.0 mg/mL by ultrafiltration on an Amicon cell (Amicon, MA) using 3000−10 000 molecular weight cutoff membranes and stored at −80 °C. Protein concentration was determined by the Lowry method (*36*), by the procedure based on the Bradford method (*37*) using bovine serum albumin as a standard, and by the experimentally determined extinction coefficient of $p13^{suc1}$ ($E_{280}^{1\%} = 17.20$).

Preparative gel filtration chromatography was performed on Sepharose CL6B and Sephacryl S-100HR (Amersham-Pharmacia Biotech AB, Uppsala, Sweden) columns (80 × 2 cm, flow rate 0.1 mL/min) eluted with a buffer containing 50 mM Tris-HCl, 2 mM EDTA, and 150 mM NaCl at pH 8.0 and using a BioLogic LP (Bio-Rad Laboratories) apparatus. Analytical size-exclusion chromatography (FPLC) was performed on a BioLogic System (Bio-Rad Laboratories) using a Bio-Silect 125-5 column eluted with a buffer containing 100 mM potassium phosphate and 150 mM NaCl at pH 6.8 at a flow rate of 0.8 mL/min. Thyroglobulin (670 kDa), IgG (158 kDa), ovalbumin (44 kDa), myoglobin (17 kDa), and vitamin B_{12} (1.35 kDa) from Bio-Rad Laboratories were used as molecular mass standards. Following size-exclusion chromatography the identity of the eluted peaks was confirmed by 13% SDS−PAGE (w/v) (*38*).

Site-Directed Mutagenesis. $p13^{suc1}$ mutants were obtained by a PCR-based site-directed mutagenesis method (*39*) using the Quick-Change PCR kit (Stratagene). By that procedure, a valine was used to replace the conserved proline residues, P90 and P92, to give the mutants P90V, P92V, and P90V/P92V. Valine was used because its mass is very close to that of proline, 99.14 vs 97.12 Da (*40*) and after trials using the option SUGMUT of the WHATIF software program (G. Vriend, Center for Molecular and Biomolecular Informatics, CMBI, Nijmengen, The Netherlands). The oligonucleotides used for P90V, P92V, and P90V/P92V were respectively 5′TATGAAGTCCATGTCGTGGAGCCACACATCCTG3′, 5′CAGGATGTGTGGCTCCACGACATGGACTTCATA3′, 5′GAAGTCCATGTCCCAGAGGTGCACATCCTGCTATTTAAG3′, 5′CTTAAATAGCAGGATGTGCACCTCTGGGACATGGACTTC3′, 5′CATGTCCATGTCGTGGAGGTGCACATCCTGCTA3′, and 5′TAGCAGGATGTGCACCTCCACGACATGGACATG3′. Mutant plasmids were identified by sequencing.

Fluorescence Measurements and Data Analysis. Steady-state fluorescence intensities and emission spectra were recorded using a PTI QuantaMaster C60/2000 spectrofluorometer with excitation and emission slit widths of 2.5 nm each and an excitation wavelength of 295 nm. The center of mass (COM) of fluorescence emission spectra was calculated as $\mathrm{COM} = \sum x_k y_k / \sum y_k$, where x and y indicate, from left to right, the kth wavelength and intensity coordinate of the emission spectrum, respectively.

Fluorescence quenching measurements of the $p13^{suc1}$ proteins were performed using potassium iodide as quencher. Protein samples at increasing concentrations of the quencher were prepared by adding small aliquots from a concentrated solution of KI (4 M). KI stock solutions were freshly prepared in the presence of $\approx 1 \times 10^{-4}$ M $Na_2S_2O_3$ to avoid I_3^- formation (*41*).

The steady-state fluorescence data were analyzed according to the general form of the Stern−Volmer equation for collisional quenching (*41*, *42*):

$$F_0/F = 1 + K_{SV}[Q] \quad (1)$$

where F_0 and F are the fluorescence intensities measured in the absence and the presence of the quencher, K_{SV} is the Stern−Volmer constant, and [Q] is the quencher concentration. This simple form of the equation was used to analyze the experimental data when linear Stern−Volmer plots were obtained. Moreover, K_{SV} is equal to $k_q\tau_0$, where k_q is the apparent rate constant for the collisional quenching process and represents a measure of the overall accessibility of the fluorophores. Alternatively, when nonlinear Stern−Volmer plots were obtained, the following modified form was used (*43*):

$$\frac{F_0}{F} = \left[\sum_{i=1}^{n} \frac{f(i)}{\{1 + K_{SV}(i)[Q]\}}\right]^{-1} \quad (2)$$

Here, the dynamic quenching of multiple species with distinct contributions, $f(i)$, and quenching constants, $K_{SV}(i)$, is considered, and the experimental data were fitted to the equation using a nonlinear least-squares procedure.

Nanosecond time-resolved fluorescence measurements were obtained by the time-correlated single photon counting method (*42*) using a Model 5000U fluorescence lifetime spectrometer (IBH Consultants Ltd., Glasgow, U.K.) implemented to perform automated multiple emission wavelength decay measurements. The instrument response function was typically 1.4 ns (FWHM) using a Hamamatzu R3235 photomultiplier. The channel width was 0.103 ns per channel, and data were collected in 1024 channels.

The data were analyzed by the nonlinear least-squares method assuming the fluorescence decay as a sum of discrete exponential components, each described by a decay constant (lifetime, τ_i) and its relative contribution (amplitude, α_i) to the total fluorescence decay (*44*):

$$I(t) = \sum \alpha_i e^{-t/\tau_i} \quad (3)$$

Decay curves collected at multiple emission wavelengths were simultaneously analyzed by the global procedure with linking lifetimes and used to resolve the decay-associated spectra (DAS) (*45*). The same method was used to analyze the fluorescence intensity decay as a function of denaturant concentrations. In this case, the lifetimes were linked within the entire concentration interval. When data were corrected for scattered light, a very short decay component (0.01 ns) was added to the fluorescence decay model. The quality of the fitting statistics was judged by the plot of the weighted residuals, the autocorrelation function of the residuals, and the value of the reduced Chi square (χ^2) (*46*). Errors associated with the recovered decay parameters (at the 67%

confidence level) were calculated using rigorous error analysis as described elsewhere (*47*).

Equilibrium Unfolding Measurements and Data Analysis. To monitor the unfolding transition of p13^{suc1} as a function of GuHCl concentration, small aliquots (25−1500 μL) of denaturant from a 8 M stock solution were added by microsyringe to a protein sample (−1 μM) of the initial volume of 2 mL. The samples were equilibrated at 25 °C before the entire emission spectrum was recorded. Data were corrected for dilution as $F_{cor} = F_{obs}(V_t/V_i)$, where F_{cor} and F_{obs} indicate the dilution-corrected and the observed fluorescence intensities, V_i represents the initial sample volume in the absence of denaturant, and V_t represents the total sample volume after the denaturant addition. Alternatively, equilibrium denaturation experiments were also performed by adding the same amount of a protein stock (100 μL) to denaturant solutions of the same volume (1.9 mL) and increasing concentrations. The results obtained by the two methods were superimposed. Each protein unfolding curve was repeated at least three times, and the error associated to the measured fluorescence intensities did not exceed 2−5%.

To describe a two-state transition, N ⇆ U, between the native and the unfolded states with an unfolding equilibrium constant, $K_{un} = [U]/[N]$, and a free energy change given by

$$\Delta G^\circ_{un} = -RT \ln K_{un} \quad (4)$$

the following linear relationship (linear extrapolation model) was used to describe the thermodynamics of the denaturant-induced unfolding of proteins (*48*, *49*):

$$\Delta G^\circ_{un} = \Delta G^\circ_{0,un} - m[D] \quad (5)$$

where $\Delta G^\circ_{0,un}$ is the free energy change of unfolding extrapolated to zero denaturant concentration at a reference temperature and m, the denaturant concentration index, is a measure of the dependence of ΔG°_{un} on denaturant concentration. A simple extension of these relationships was used to describe a three-state transition, N ⇆ I ⇆ U, where I is an intermediate state and the equilibrium constants of each unfolding step can be defined as $K_{I/N} = [I]/[N]$ and $K_{U/I} = [U]/[I]$, respectively.

Equilibrium denaturation data analysis was performed as previously described (*49*). Briefly, from the combination of eqs 4 and 5 and using the appropriate partition coefficients to indicate the mole fractions of each state, the following equation was used to fit the experimental data by a two-state transition model (*49*):

$$F = \frac{F_{0N} + S_N[D] + (F_{0U} + S_U[D])e^{(-\Delta G^\circ_{0,un} + m[D])/RT}}{1 + e^{(-\Delta G^\circ_{0,un} + m[D])/RT}} \quad (6)$$

where F_{0N} and F_{0U} are the intensities of the native and the unfolded states in the absence of the denaturant D, and the terms S_N and S_U represent the baseline slopes for the native and unfolded regions. When reported, the experimental data were also analyzed according to a three-state transition model using an expansion of eq 6 which contemplated a total number of 10 fitting parameters. In this case, with $\Delta G^\circ_{0,un1}$ and $\Delta G^\circ_{0,un2}$ were indicated the free energy changes in the absence of denaturant for the N ⇆ I and the I ⇆ U denaturation reaction pathways, respectively.

Equation fitting was obtained by the nonlinear least-squares utility included in the SigmaPlot 3.2 software package (SPSS Science Software, Germany).

RESULTS

p13^{suc1} wild type is known to exists in a monomer and a dimer form in a very slow equilibrium, with the monomer largely representing the predominant species (70−80%), and they have been suggested to be separated by a high thermodynamic barrier (*34*).

The structural basis of the oligomeric species is an arm exchange between β-hinge chains as shown by crystallographic data (*23*−*25*). To investigate the role of this region by solution methods, different mutants of the β-hinge proline residues, P90V, P92V, and P90V/P92V, were prepared, and their properties were studied by biochemical and biophysical techniques.

Oligomerization Properties of Wild-Type and Mutant p13^{suc1} Proteins. The ability to form oligomeric species of the wild type and the proline to valine mutants of p13^{suc1} was investigated by gel filtration chromatography and SDS−PAGE. The results obtained are summarized in Figure 2.

From Sepharose CL6B chromatography (Figure 2A), the wild-type protein (left side panels) eluted as a mixture of monomer and dimer species. This is a well-known pattern (*28*, *30*, *34*) and was revealed by SDS−PAGE analysis of the fractions collected from this separation (Figure 2B) that showed the presence of the native protein under two distinct elution volumes. These volumes were separately collected in two pools: a first pool contained fractions 50−70 and the second pool contained fractions 71−83. In Figure 2C, it is shown the following elution of the first p13^{suc1}-containing pool loaded on Sephacryl S-100HR. With the dashed line is marked the elution of the second pool. The chromatogram clearly showed the separation of the wild-type protein in two stable monomer (M) and dimer (D) peaks. With the single mutant P92V equivalent results were obtained (see below), thus indicating that substitution on this position does not significantly affect arm-exchange dimerization. On the other hand, with the single mutant P90V (Figure 2, right side panels) we could not detect the presence of the dimer form, and the protein was found exclusively in a single elution volume. These results, obtained with the valine mutants of Pro-90 and Pro-92, remarkably reproduced the findings obtained by Rousseau et al. (*31*) with alanine mutants and indicated the Pro-90 residue as the determinant in triggering the CKS dimerization by domain swapping. The final separation of the double mutant P90V/P92V was consistent with this interpretation, and only the monomer form was isolated.

To further characterize the expressed SUC1 variants, samples of the different mutant products were tested by analytical size-exclusion chromatography. In Figure 3, the elution profile of a sample of the wild-type protein predominantly in the dimer form (line 1) is shown together with samples of P90V (line 2), P92V (line 3), and P90V/P92V (line 4). The small amount of the monomer form in the wild-type chromatogram clearly indicated the correspondence of the retention time of the P90V and P90V/P92V samples with that of the monomer form. Finally, the size-exclusion separation of the P92V sample clearly shows that this protein elutes as a mixture of monomer and dimer forms.

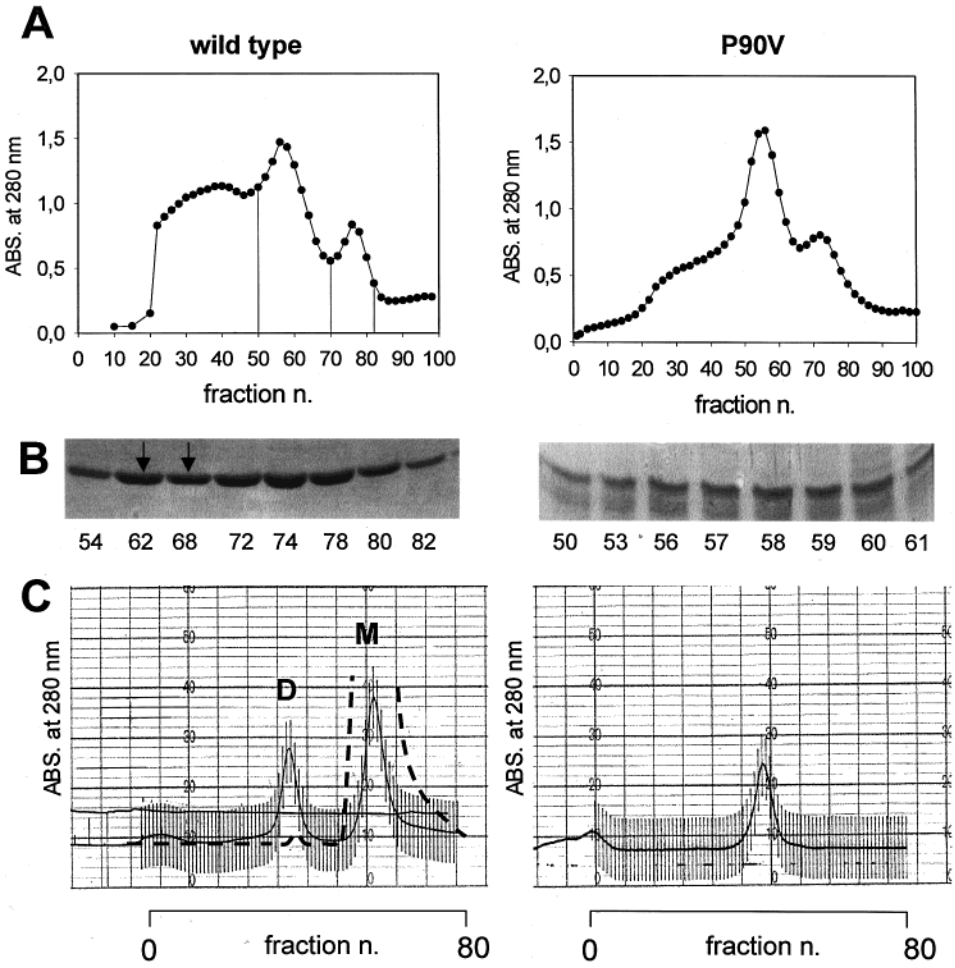

FIGURE 2: Gel filtration purification and SDS−PAGE analysis of the p13^{suc1} wild-type and P90V proteins. (A) Preparative separation on Sepharose CL6B. The column was equilibrated and eluted (flow rate 0.3 mL/min) with 50 mM Tris-HCl and 150 mM NaCl at pH 8.0 containing 2 mM EDTA. The vertical lines indicate the collected pools (see text). (B) SDS−PAGE (13%) analysis of the fractions collected from the Sepharose CL6B elution. Black arrows indicate a higher stain density in fraction 62 (dimer) than in fraction 68, with the highest protein concentration found in fraction 74 (monomer). (C) Final preparative separation on Sephacryl S-100 HR (see text). The column was equilibrated and eluted using the same buffer reported for the Sepharose CL6B column (flow rate 0.1 mL/min). The UV range scale of the detector was set to 0.5 AU, and a 280 nm band-pass filter was used.

Steady-State Fluorescence-Detected Equilibrium Denaturation of Wild-Type and Mutant p13^{suc1} Proteins. The steady-state intrinsic fluorescence properties of p13^{suc1} have been previously characterized and the emission of its tryptophan residues, Trp-71 and Trp-82, used to obtain structural and hydrodynamics information (*35*). In its native form the emission spectrum of p13^{suc1} is centered at 336 nm, and upon denaturation it shifts to 355 nm with 70% decrease of the fluorescence intensity. These changes have been used to monitor the denaturation of p13^{suc1} and to show that it unfolds reversibly using guanidine and urea (*31*, *35*). In addition, the unfolding kinetic properties of the dimeric form have been shown to be nearly identical to those of the monomer, and it has been concluded that, with the exception of the β-hinge region, the two forms have essentially the same structure and the same energy barrier of unfolding (*31*).

In this work equilibrium denaturation studies were carried out to examine the structural stability and thermodynamics of the p13^{suc1} wild type and its variant proteins and, in particular, to study the role of the β-hinge region and its proline residues on the unfolding transition. In Figure 4 A, equilibrium denaturation experiments monitored by fluorescence intensity measurements are presented. With increasing denaturant concentration the wild-type protein unfolded with a transition that was appropriately fitted by a typical two-state equation. The same experiment is reported also for the single point mutations P90V and P92V and for the double mutation P90V/P92V. It is shown that the two-state unfolding mechanism of the wild-type protein was conserved when the single proline-mutated proteins were assayed. In addition, the recovered thermodynamic parameters reported in Table 1 reflected a small shift of the denaturation curve of P90V to a higher GuHCl concentration (C_m 1.96 M vs 1.80 M) and a lower denaturant index (m_{GuHCl} 3.42 kcal mol^{-1} M^{-1} vs 4.08 kcal mol^{-1} M^{-1}), whereas the denaturation curve of P92V did not significantly differ from that obtained with the wild-type protein. On the other hand, with the double mutant the denaturation curve showed a more complex transition. Indeed, the unfolding transition could not be satisfactorily described by a two-state reaction (dashed line), and a three-state model was required to obtain a good fit of the experimental data (solid line). According to the thermodynamic parameters reported in Table 1, this transition was consistent with the formation of an intermediate state at low GuHCl concentrations ($\Delta G°_{0,un1}$ 1 kcal mol^{-1} and a C_{m1} 0.7 M) whose contribution to the overall protein unfolding corresponded to a mole fraction of 0.15, calculated as $\Delta G°_{0,un1}/(\Delta G°_{0,un1} + \Delta G°_{0,un2})$.

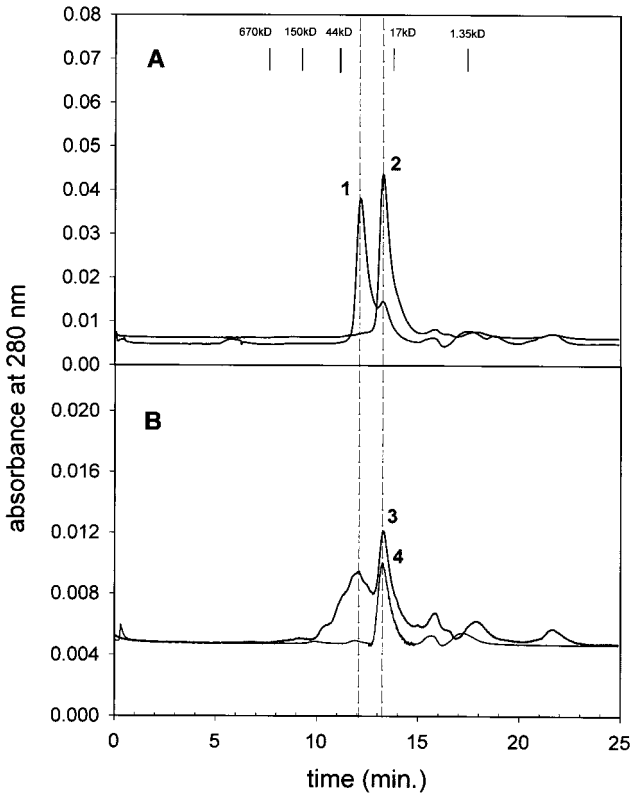

FIGURE 3: Analytical size-exclusion chromatography of wild-type and mutant p13^{suc1} proteins. (A) Chromatograms 1 and 2 refer to the injection (250 μL) of a sample (0.2 mg/mL) of purified p13^{suc1} wild-type dimer and P90V, respectively. (B) Chromatograms 3 and 4 refer to the injection of a sample of P92V and P90V/P92V from a Sepharose CL6B separation, respectively. A Bio-Silect 125-5 Bio-Rad FPLC column was used with a buffer containing 100 mM potassium phosphate and 150 mM NaCl at pH 6.8 as the mobile phase (flow rate of 0.8 mL/min). The elution positions of molecular mass standards are indicated by vertical bars.

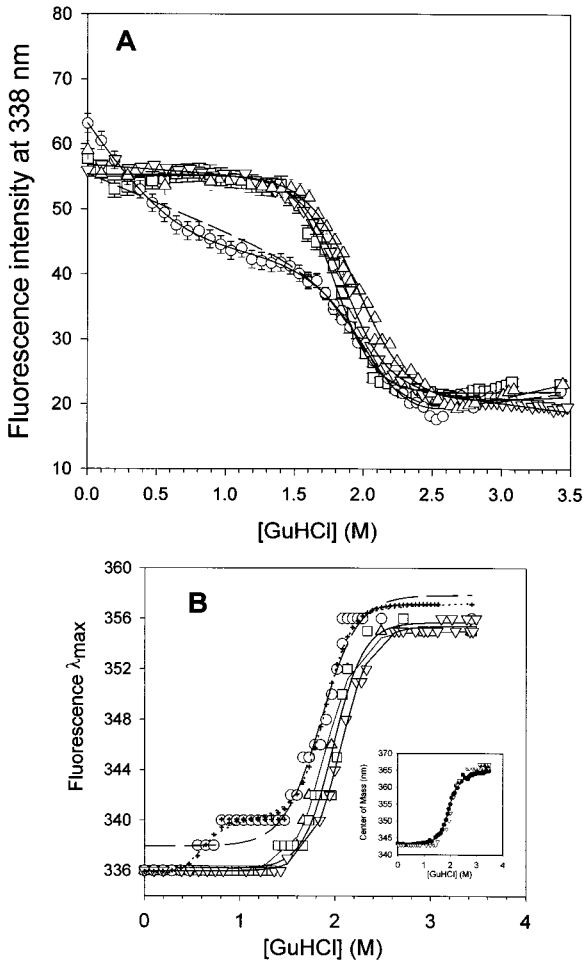

FIGURE 4: Equilibrium unfolding transitions of p13^{suc1} wild-type and mutant proteins by GuHCl. (A) Steady-state fluorescence intensity changes as a function of the denaturant concentration of the wild type (□) and P90V (△), P92V (▽), and P90V/P92V (○) mutants using GuHCl. The protein (0.8 μM) was dissolved in 50 mM Tris-HCl, pH 7.1, and 50 mM NaCl at 25 °C. Emission spectra were recorded exciting at 295 nm and using excitation and emission slit widths of 2.5 nm. (B) Changes of the λ_{max} of the emission spectra of the p13^{suc1} proteins as a function of the denaturant concentration. In the insert, the transitions obtained with the mutant P92V by the changes of the center of mass (●) and λ_{max} (▽) are shown. For comparison with the data presented in Table 1, the relative center of mass recovered thermodynamic parameters were the following: $\Delta G^{\circ}_{0,un1} = 6.89 \pm 0.33$ (kcal mol^{-1}), $m_{GuHCl1} = 3.59 \pm 0.17$ (kcal mol^{-1} M^{-1}), and $C_{m1} = 1.92 \pm 0.13$ (M). In the panels, solid lines represent the nonlinear least-squares fits of the p13^{suc1} wild-type and single mutant data to a two-state equation and that of the double mutant data to a three-state equation; the dashed lines represent the results obtained with the double mutant using a two-state equation, whereas the dotted line indicates the result obtained using a three-state equation. With the cross symbols are indicated the resulting fitting functions of the experimental data analyzed as two independent two-state transition steps (model "2+2" of Table 1).

The dependence of the emission spectral distribution on the chemical nature of the fluorophore's surrounding is an essential quality of many fluorescent probes including tryptophan (*42*). Thus, the unfolding reactions of the p13^{suc1} proteins were also monitored by the changes of the position of the tryptophan emission spectra. Although the calculation of the center of mass is largely the preferred measure of this property, we found that, apart from a difference in the recovered coordinate (COM = 343 nm vs λ_{max} = 336 nm, under native conditions), the final results obtained by this procedure did not significantly differ from those obtained by recording simply the changes of the position of the maximum of the emission intensity (λ_{max}). For this reason, to analyze repeated experimental data of the different mutants' transitions, we made use of the latter more expeditious method. Such results are presented in Figure 4B, where in the insert graphically superimposed transitions obtained by COM calculations and λ_{max} measurements are also presented for comparison. It is shown that the fluorescence λ_{max}-detected unfolding transitions of the wild-type, P90V, and P92V proteins were nearly superimposed. Proper fittings of the experimental data to a two-state model were obtained, and the emission wavelengths associated to the initial and the final states of the unfolding transition were correctly recovered from these analyses. On the contrary, the maximum of the fluorescence emission of the P90V/P92V protein shifted to the red region of the spectrum at lower GuHCl concentrations (C_m 1.67 M vs 1.98 M), and the fitting of the experimental data to a two-state model failed to recover the emission wavelengths characteristic of the initial and the final states of the unfolding transition (dashed line in Figure 4B). These data were also analyzed in terms of a three-state transition. Although by this model a fitting function that better traced the experimental curve was found (dotted line), the presence of 10 fitting parameters likely caused large errors, and not unique solutions for the searched parameters were obtained (data not reported). As an alterna-

Table 1: Thermodynamics of the Equilibrium Unfolding Transition of the p13^{suc1} Proteins[a]

protein	model	$\Delta G°_{0,un1}$	C_{m1}	m_{GuHCl1}	$\Delta G°_{0,un2}$	C_{m2}	m_{GuHCl2}
			Changes of the Fluorescence Intensity[b]				
wild type	2	7.34 ± 0.35	1.80 ± 0.12	4.08 ± 0.20			
P90V	2	6.71 ± 0.18	1.96 ± 0.08	3.42 ± 0.10			
P92V	2	7.16 ± 0.18	1.86 ± 0.10	3.85 ± 0.10			
P90V/P92V	2	6.97 ± 0.81	2.04 ± 0.35	3.42 ± 0.41			
P90V/P92V	3	1.25 ± 0.81	0.74 ± 0.70	1.70 ± 1.40	7.08 ± 1.02	2.08 ± 0.42	3.39 ± 0.46
			Changes of the Fluorescence λ_{max}[c]				
wild type	2	7.36 ± 0.57	1.98 ± 0.21	3.72 ± 0.29			
P90V	2	6.74 ± 0.90	1.90 ± 0.27	3.55 ± 0.48			
P92V	2	7.28 ± 0.54	2.05 ± 0.20	3.55 ± 0.25			
P90V/P92V	2	5.52 ± 0.40	1.67 ± 0.17	3.31 ± 0.25			
P90V/P92V	2+2	3.86 ± 0.95	0.64 ± 0.22	6.05 ± 1.43	7.80 ± 0.81	1.88 ± 0.28	4.14 ± 0.44

[a] $\Delta G°_{0,uni}$ (kcal mol^{-1}), the free energy change of unfolding extrapolated to 0 M GuHCl concentration, and m_{GuHCli} (kcal mol^{-1} M^{-1}), the dependence of $\Delta G°_{uni}$ on denaturant concentration, were obtained from the nonlinear least-squares fitting of the data presented in Figure 4. In the table, according to the two-state transition N ⇆ U (model 2) with $\Delta G°_{0,un1}$ and m_{GuHCl1} are represented the relative parameters $\Delta G°_{0,U/N}$ and $m_{U/N}$, whereas according to the three-state transition N ⇆ I ⇆ U (model 3) with $\Delta G°_{0,un1}$, $\Delta G°_{0,un2}$, m_{GuHCl1}, and m_{GuHCl2} are represented the relative parameters $\Delta G°_{0,I/N}$, $\Delta G°_{0,U/I}$, $m_{I/N}$, and $m_{U/I}$, respectively. C_{mi} (M), the GuHCl concentrations at half-denaturation, were obtained as $C_{mi} = \Delta G°_{0,uni}/m_{GuHCli}$. The errors in $\Delta G°_{0,uni}$ and m_{GuHCli} were recovered from the nonlinear least-squares analysis; those in C_{mi} were obtained from the relative propagation of errors (*46*). [b] The changes of the fluorescence intensity as a function of the GuHCl concentration were measured by exciting the samples at 295 nm and observing the emission at 338 nm and using excitation and emission slit widths of 2.5 nm each. [c] The changes in the maxima of the tryptophan emission spectra were measured under the same conditions reported above. The contribution of the blank was subtracted from the recorded spectra at all GuHCl concentrations. The emission λ_{max} (nm) for the native and the denatured states recovered from the nonlinear analysis were as follows: wild type, 336.2 and 355.7; P90V, 336.0 and 355.3; P92V, 336.6 and 354.8; and P90V/P92V, 337.9 and 357.9. When the complex transition of the double mutant was analyzed as two independent two-state transitions (model 2+2), the emission λ_{max} (nm) recovered by the one-at-a-time fitting were as follows: first step, 335.9 and 340.1; and second step, 340.1 and 357.1.

tive, the entire complex transition was considered as two "independent" two-state transitions, and the [GuHCl] regions (0−1.4 and 0.8−3.4 M) were separately analyzed. This approach provided meaningful thermodynamic parameters with C_{mi} comparable to those recovered by fluorescence intensity measurements (Table 1). Thus, the information provided by the precocious increase of the emission λ_{max} of this double mutant is relevant. In the lower denaturant concentration interval, it reported the contribution to the unfolding process of an intermediate species with higher accessibility of the tryptophan residues to the polar solvent.

Altogether, these results indicate that the Pro-90 residue is the determinant for the domain swapping dimerization mechanism and a crucial role is played by both of the proline residues of the β-hinge since their concomitant substitution significantly affects the unfolding transition of p13^{suc1}.

Time-Resolved Fluorescence-Detected Equilibrium Denaturation of Wild-Type and Mutant p13^{suc1} Proteins. In a preceding report (*35*) the fluorescence decay of wild-type p13^{suc1} under native conditions has been resolved in two major decay components of 2.9 ns (τ_2) and 6.0 ns (τ_3) which contributed 96% of the total emitted fluorescence (τ_2 = 32%; τ_3 = 64%), with the residual fluorescence due to a fast component of 0.6 ns (τ_1). In addition, each fluorescence lifetime spectral distribution (DAS) has been defined. The value of this methodology for understanding the photophysical heterogeneity of proteins has been exhaustively described (*45*, *50*), and it has provided relevant information to study the conformational dynamics and changes of the local secondary structure of proteins in many biological systems (*51*−*54*). Here, the DAS of the wild-type protein and its mutants were resolved to define the nature of the molecular contour of the tryptophan residues of each p13^{suc1} variant in its native state. An example of these data is presented in Figure 5, where the recovered spectra for the wild type and the double mutant are shown. In the absence of significant changes of the recovered lifetime values (see legend to Figure 5), they suggest that in the native state the environment of the tryptophan residues was not significantly affected by substitution of the prolines in the β-hinge chain.

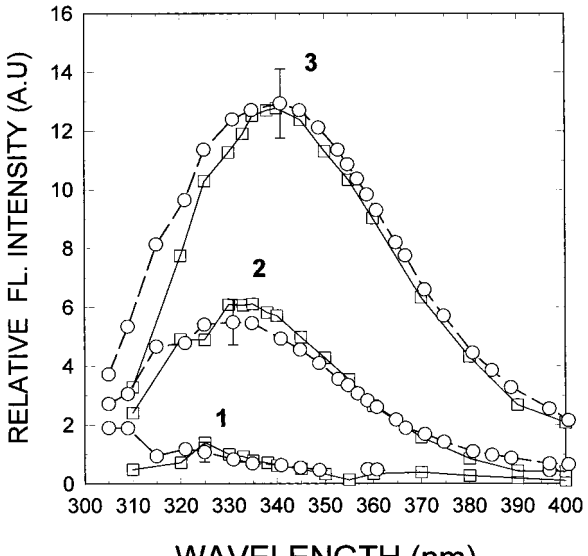

FIGURE 5: DAS of p13^{suc1} wild type and P90V/P92V. DAS of native wild-type (□) and P90V/P92V (○) p13^{suc1} (0.2 mg/mL in 50 mM Tris-HCl, pH 8.0, 2 mM EDTA, 20 °C). Data were collected using an excitation wavelength of 295 nm. The DAS were obtained from the global analysis of multiple emission wavelength experiments (16−24 data sets). With 1, 2, and 3 are indicated the spectra (expressed as $\alpha_i\tau_i$ products) associated with τ_1, τ_2, and τ_3, respectively. The recovered decay parameters with the relative upper and lower limits (at the 67% confidence level) of wild-type p13^{suc1} were $\alpha_1 = 0.13 < 0.21 < 0.32$, $\tau_1 = 0.42 < 0.76 < 1.24$, $\alpha_2 = 0.28 < 0.36 < 0.42$, $\tau_2 = 1.97 < 2.76 < 3.87$, $\alpha_3 = 0.26 < 0.39 < 0.48$, $\tau_3 = 5.43 < 5.74 < 6.18$, whereas the recovered parameters of P90V/P92V were $\alpha_1 = 0.14 < 0.20 < 0.24$, $\tau_1 = 0.14 < 0.25 < 0.39$, $\alpha_2 = 0.21 < 0.25 < 0.31$, $\tau_2 = 2.31 < 2.79 < 3.40$, $\alpha_3 = 0.21 < 0.29 < 0.35$, $\tau_3 = 5.28 < 5.58 < 5.95$. Global reduced χ^2 ranged from 1.13 to 1.33.

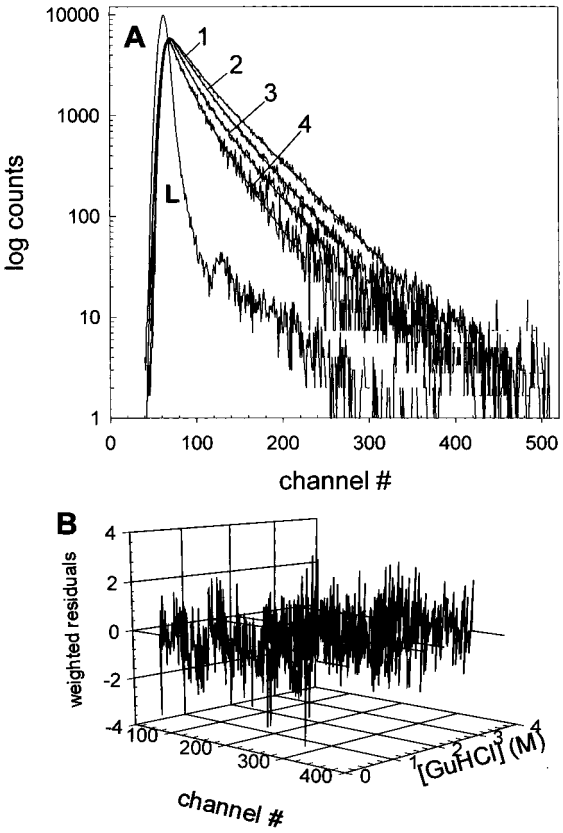

FIGURE 6: Time-resolved fluorescence decay of p13^{suc1} wild type as a function of GuHCl concentration. (A) Typical fluorescence decay data obtained at 25 °C using an excitation wavelength of 295 nm (slit width of 32 nm) and observing the fluorescence emission at 338 nm (slit width of 16 nm). The protein concentration was 0.2 mg/mL in a buffer containing 50 mM Tris-HCl and 50 mM NaCl (pH 7.1) at 0 M (curve 1), 1.6 M (curve 2), 2.07 M (curve 3), and 3.50 M (curve 4) GuHCl concentrations. The calibration time for each channel was 0.103 ns. On the *Y*-axis the photon counts are reported in a logarithmic scale. With L the instrument's response function (lamp) is reported, whereas the slower decaying noisy and noise-free solid curves represent the experimental decay and the theoretical parameters convolved with the lamp, respectively. Decay curves are reported normalized to the maximum count peak of the experiment recorded in the absence of GuHCl. (B) Plot of the weighted residuals obtained from the analysis of the data reported above according to a biexponential model plus a scatter component. χ^2 from single decay curve analysis ranged from 0.99 to 1.27.

Upon denaturation of wild-type p13^{suc1}, no significant changes of the lifetimes were observed, with the decrease of the fluorescence intensity that was assigned to a drop of the amplitude of the long lifetime (α_3) and a concomitant increase of the amplitude of the medium (α_2) and the short lifetime (α_1) (*35*). Thus, lifetime amplitudes were found as reliable markers of the protein unfolding. Here, because of the low relative yield of the shortest component (4%) and the consequent higher variability associated to its amplitude, we monitored the equilibrium denaturation of the p13^{suc1} proteins by examining the changes in the amplitudes of the two major decay components, α_2 and α_3. In Figure 6, typical experimental data recorded in the absence and in the presence of three increasing GuHCl concentrations are shown together with the plot of the relative weighted residuals obtained by the analysis of the fluorescence decays as biexponential function plus a scattering component. The results of the entire array of the decay experiments collected as a function of

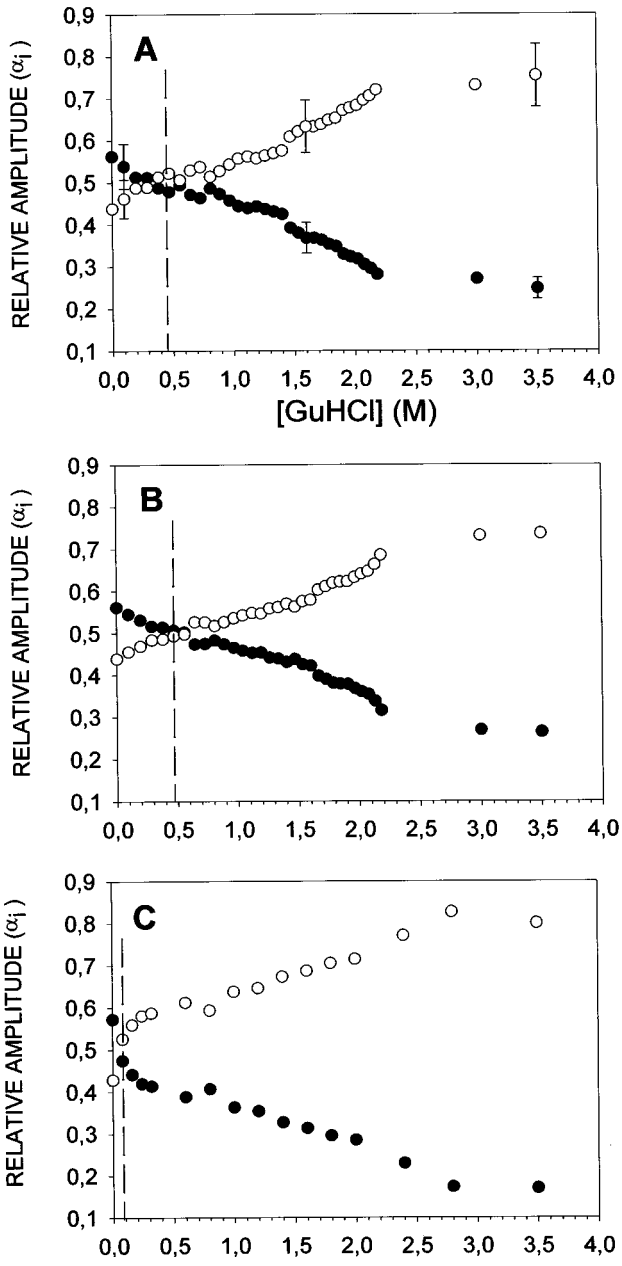

FIGURE 7: Time-resolved fluorescence equilibrium denaturation of p13^{suc1} wild-type and mutant proteins. Plot of the recovered relative amplitudes, α_2 (○) and α_3 (●), of the intrinsic fluorescence decay of wild-type (A), P90V (B), and P90V/P92V (C) p13^{suc1} as a function of GuHCl concentration. Decay curves were collected up to 10 000 counts in the peak, and they were analyzed by the global procedure by linking the lifetimes across the entire denaturation transition.

GuHCl concentrations are presented in Figure 7. They show that the wild type and the single mutant P90/V share a similar crossing point (0.5 M GuHCl) of the α_2 and α_3 amplitudes. On the other hand, with P90V/P92V this event took place at much lower GuHCl concentrations, confirming in the nanosecond time domain that (1) the structural changes involved affect the tryptophan environment and that (2) with double mutation, considerable conformational degeneracy was induced at very low levels of denaturant.

Structure Accessibility of Wild-Type and Mutant p13^{suc1} Proteins at Low GuHCl Concentration. Fluorescence quenching measurements provide a tool to investigate the solvent accessibility of intrinsic and extrinsic fluorophores in proteins

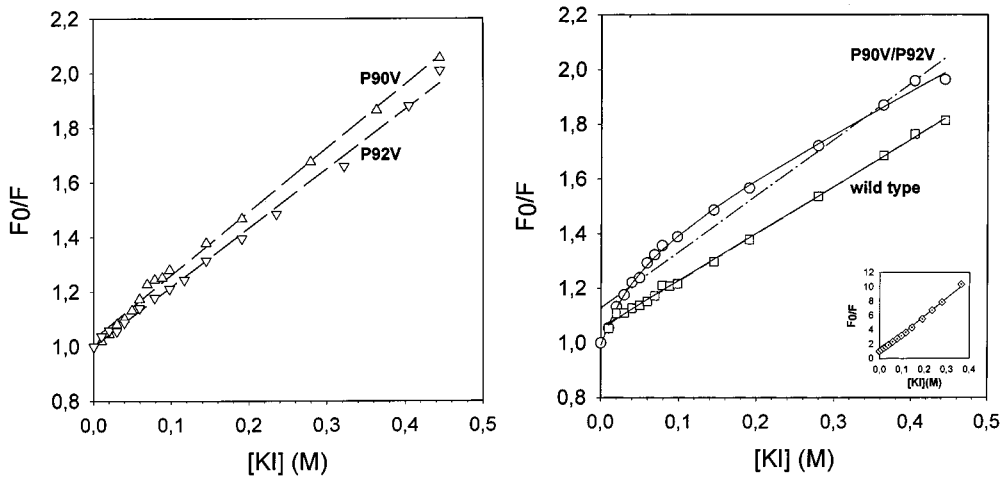

FIGURE 8: Stern−Volmer plots of p13^{suc1} wild- type and mutant proteins obtained in the presence of 1 M GuHCl. Steady-state fluorescence intensity measurements were performed at 22 °C using an excitation wavelength of 295 nm and observing the emission at 340 nm. The protein samples (1 μM) were dissolved in a buffer containing 50 mM Tris-HCl and 50 mM NaCl (pH 7.1), and small aliquots of KI (4 M) were added by microsyringe. In the left and the right panels, the results obtained with P90V (Δ), P92V (▽), wild-type (□), and P90V/P92V (○) p13^{suc1} are presented, respectively. With the dashed lines are represented the results obtained by the linear regression fits and with the solid lines are represented the results obtained by the nonlinear least-squares fits of the experimental data. The dot-dashed line represents the results of the linear regression fit obtained with P90V/P92V. The quenching of melatonin measured under the same conditions is reported in the insert of the right panel.

(*42*). According to the Stern−Volmer treatment of steady-state fluorescence quenching data (see eq 1), a linear plot is expected to describe purely collisional quenching processes, and it reflects the existence of a population of fluorophores with equivalent accessibility. Nonetheless, nonlinear plots have been often described, and in the common case of a downward curvature these graphs have been related to the existence of multiple emitting species with distinct accessibilities (i.e., tryptophan residues located in distinct regions of the same protein or a mixture of proteins in solution with significantly different solvent accessibility) (*41*, *42*). In addition, methods have been developed to separate the specific contribution of each species to the overall quenching process (*41*−*43*).

From the general representation of unfolding intermediate states of globular proteins (i.e., a molten globule) (*55*), the presence of highly solvent-accessible hydrophobic regions would distinguish these states from the native structure. Here, by fluorescence quenching measurements on the different p13^{suc1} products we aimed to unravel distinct protein accessibilities and, in particular, to test by this technique the formation, at low denaturant concentrations, of intermediate states of the P90V/P92V mutant. Quenching experiments were carried out at 1 M GuHCl and using KI as a quencher. In the left and the right panels of Figure 8 the Stern−Volmer plots obtained with the p13^{suc1} wild-type protein and its variants are presented. The relative quenching constants recovered by linear regression and nonlinear least-squares analyses of the experimental data are shown in Table 2. As reported in Figure 8, linear fits well described the collisional quenching of the wild-type and the single mutant proteins. The recovered quenching constants (K_{SV1}) ranged from 1.8 to 2.3 M^{-1}, in good agreement with the value of 2.09 M^{-1} previously measured by time-resolved techniques for the total collisional quenching of p13^{suc1} under native conditions (*35*). Thus, the quenching of these p13^{suc1} products was consistent with the existence of a single population of protein molecules with low solvent accessibility and nativelike structure. However, the linear regression analysis was clearly inadequate to describe the collisional quenching of the double mutant protein as shown by the dot-dashed line in the right panel of Figure 8. A nonlinear approach was required to accurately describe the data (solid line). In this case, the best result was obtained by assuming a model of two species with distinct accessibilities. According to this model, in the presence of 1 M GuHCl, the intrinsic fluorescence quenching of the double mutant P90V/P91V originated by the sum of a 70% contribution of a low solvent-accessible species (K_{SV1} = 1.0 M^{-1}) and a 30% contribution of a very high solvent-accessible species (K_{SV2} = 26.2 M^{-1}). Interestingly, the latter quenching constant was found to be very close to the value measured under the same condition with melatonin (see insert to Figure 8 and Table 2), a compound used as a model of fully exposed tryptophan residues. Moreover, when the graphs obtained with wild type and single mutants of p13^{suc1} were analyzed by the nonlinear method to test its accuracy, the recovered quenching constants did not differ significantly from the results obtained by the simple linear regression method. As an example, the quenching parameters recovered with wild-type p13^{suc1} are reported in Table 2.

Table 2: Stern−Volmer Quenching Constants of the p13^{suc1} Proteins in the Presence of 1 M GuHCl[a]

protein	f_1	K_{SV1} (M^{-1})	f_2	K_{SV2} (M^{-1})
wild type[b]	1	1.75 ± 0.17		
wild type[c]	0.94 ± 0.01	1.62 ± 0.03	0.06 ± 0.01	440 ± 597
P90V[b]	1	2.34 ± 0.20		
P92V[b]	1	2.13 ± 0.20		
P90V/P92V[b]	1	2.05 ± 0.20		
P90V/P92V[c]	0.69 ± 0.03	1.01 ± 0.15	0.31 ± 0.03	26.16 ± 6.3
melatonin[b,d]	1	25.15 ± 0.10		

[a] The quenching parameters reported refer to the experimental data presented in Figure 8. [b] Linear regression analysis was used to fit the data to eq 1 in terms of the collisional quenching of a unique species with quenching constants K_{SV1}. [c] Nonlinear least-squares analysis was used to fit the data to eq 2 in terms of the collisional quenching of multiple species. In this approach, two species were assumed with distinct quenching constants, K_{SV1} and K_{SV2} (see text). [d] Melatonin in water (OD = 0.06) was used as a model compound for the quenching of fully exposed tryptophan.

We interpret the experimental evidence obtained with the double mutant of p13^{suc1} in terms of the formation, at low denaturant concentrations, of an unfolding intermediate state with high solvent-accessible structural organization which coexists in solution with a nativelike structural form.

DISCUSSION

CKS are small proteins which act at different stages of the cell cycle. They appeared to be associated to CDK1/CDK2 (*11*, *13*, *15*) and to influence crucial events in the regulation of the biological function of these kinases. The resolution of the structure of p13^{suc1} (*22*−*24*) has provided new clues for understanding structure/function relationships of CKS. In particular, apart from a "phosphate anion-binding" site and a "hydrophobic patch" site that have been suggested as potential sites for interaction with CDC2 (*24*) and substrate recognition in the ubiquitin-mediated degradation of the cyclin B−CDC2 complex degradation (*21*), an unusual β-strand-exchanged dimer form has been revealed. This structure has been found also in the human CKS homologues (*25*, *26*), and the dimerization reaction by arm exchange has been referred to a domain swapping mechanism.

Moreover, with resolution of the CDK2−CksHs1 complex (*27*) it has been shown that the critical residues for the structural interactions in kinase binding are invariant within the CKS protein family and, conceivably, the structure of CksHs1 bound to CDK2 can be expected to be representative for both human and yeast CKS proteins. Remarkably, it has been described that, with dimerization and extension of the β-hinge, the crucial CKS residues are moved apart from interacting with the complement side chains on CDK2.

In the present work we have studied the effects of replacement of the proline residues of the β-hinge conserved sequence, HxPEPH, on the protein oligomerization and unfolding transition by integrated mutagenesis and biochemical and biophysical approaches. Moreover, it has been pointed out by Bergdoll et al. (*28*) that the presence of a pair or a triplet of prolines separated by one residue may represent a conserved sequence motif among arm-exchanged proteins (i.e., SV40, Cks, and aspartate aminotransferase). For this reason, the effect of the associated substitution of both of the proline residues has been also analyzed in the study.

Oligomerization of the p13^{suc1} Wild-Type Protein and Its Variants. The results presented here using valine to replace the β-hinge's proline residues are in excellent agreement with the alanine-screening study previously described by Rousseau et al. (*31*) where the determinant role of Pro-90 on p13^{suc1} dimerization by domain swapping was first reported. Analytical size-exclusion runs on the P90V mutant (Figure 3) unambiguously substantiated this finding.

Equilibrium Denaturation of the p13^{suc1} Wild-Type Protein and Its Variants. The fluorescence-detected denaturation curves and thermodynamics obtained with the wild-type protein and its single mutant variants have not shown remarkable differences within error (Figure 4 and Table 1), and these transitions could be strictly described by a two-state model. From this evidence it can be concluded that single substitutions of the β-hinge proline residues do not affect the cooperative character of the denaturation reaction and the recovered transitions can be appropriately described in terms of a simple equilibrium between two protein populations with native and denatured structures, as a function of GuHCl concentrations.

Notably, a different unfolding process was observed when both of the proline residues were replaced and the P90V/P92V mutant's denaturation curve was best fitted by a multistate transition model. This result is consistent with the formation of an unfolding intermediate state at low denaturant concentrations. More important, it also indicates that, in CKS, structural fluctuations and heterogeneity may be constrained by the coordinate role of Pro-90 and Pro-92.

Although the actual structure of partially folded states of globular proteins can be extremely variable (from compact intermediate, as the "molten globule", to entirely unfolded), the existence of solvent-accessible hydrophobic regions is commonly regarded as a signature of unfolding intermediate states (*55*). Leading from this concept, in the present paper some experiments have been designed to possibly distinguish the characteristic solvent accessibility and polarity of the tryptophans' environment of the double mutant from that of the single mutants and the wild-type p13^{suc1} proteins.

In addition to the changes of the fluorescence intensity (Figure 4A), denaturation curves were traced also by recording the changes of the emission λ_{max} (Figure 4B). By testing different simulation models and using photophysical arguments, Eftink (*49*) delineated potential pitfalls in monitoring unfolding transition in proteins. In particular, he pointed out that when the quantum yields of the native and the unfolded states differ significantly, then the emission spectrum of the state with a higher quantum yield will dominate and the apparent λ_{max} is skewed toward this state. The fluorescence properties of p13^{suc1} under native and denatured conditions (*35*) closely resembled the case II simulation model presented by Eftink (*49*). In this situation the quantum yield of the native state strongly dominates the quantum yield of the unfolded state and changes of the apparent λ_{max} trace transition curves that are shifted to higher denaturant concentrations (i.e., higher C_m are recovered). In this respect, the experimental C_m values obtained with wild type and P92V reported in Table 1 and their relative changes obtained using the different fluorescence methods are in excellent agreement with the simulations discussed by Eftink (*49*). More important, in the absence of significant changes of the relative quantum yields of P90V/P92V, these considerations further stress the actual structural meaning of the shift to lower [GuHCl] of the C_m calculated with this mutant. It indicates that upon double mutation a protein species with lower stability and increased polarity of the tryptophan residues' environment is formed.

This result can be relevant for understanding the overall structural organization of p13^{suc1} and CKS proteins in general. Thus, to further investigate the effect of double substitution and possibly confirm the specific induction of an intermediate state, the unfolding reaction of the p13^{suc1} proteins was assessed by time-resolved fluorescence techniques. Under native conditions, none of the different substitutions modified the basic spectral features of the DAS resolved with the wild-type protein (Figure 5). On the other hand, upon the denaturant perturbation and using the changes of the intrinsic fluorescence decay amplitudes (α_2 and α_3) of the p13^{suc1} proteins as "markers" of unfolding (*35*), a significant

deviation of the data obtained with P90V/P92V from the data obtained with wild-type and single mutant proteins was observed (Figure 7). Namely, the increase of α_2 and the decrease of α_3 took place at a much lower denaturant concentration. Hence, in good agreement with the steady-state measurements, the resolution of dynamics parameters in the nanosecond time scale has confirmed the relevant structural role of the proline pair and how, solely, their associate replacement affects the whole CKS protein stability.

Moreover, as mentioned under the Results section, changes of the preexponential terms of the emission decay of tryptophan have been used to study structural properties of proteins in biological systems as different as isolated molecules (*52*, *53*) and protein−DNA (*54*), and peptide−lipid membrane (*55*) complexes. In general, changes of the fluorescence lifetime amplitudes can be regarded as a change of the contribution of distinct rotamer populations (conformers) (*52*, *53*) or as a change of the contribution of a specific tryptophan residue to the overall protein conformation. With $p13^{suc1}$, it has been shown previously that the intrinsic emitted fluorescence is dominated by the contribution of the two tryptophan residues, and the more realistic explanation of its multiexponential decay is a simple two-compartment heterogeneity model (*35*). In addition, the amplitude α_2 was assigned to Trp-82 and the amplitude α_3 was assigned to Trp-71. These two aromatic residues are located at the NH_2 extreme of β-strand 3 and at the COOH extreme of α-helix 3, respectively. Therefore, it appears that modifications on the β-hinge sequence can affect the structural stability and organization of peptide chains several residues apart. In particular, lifetime tryptophan residue assignments (*35*) took advantage also of the location of Trp-82 inside the phosphate anion-binding site (*24*). Thus, it would be tempting to postulate that β-strand organization affects the tridimensional structure of such a biologically relevant site of CKS.

Steady-State Fluorescence Quenching Measurements and Structure Accessibility of the $p13^{suc1}$ Wild-Type Protein and Its Variants. Fluorescence quenching techniques can provide the quantitative resolution of diffusional rates and useful information on the solvent accessibility of proteins (*42*). Here, Stern−Volmer plots were obtained at 1 M GuHCl to compare and evaluate the accessibility of the $p13^{suc1}$ proteins to a soluble quencher (KI). Yet, the linear graphs obtained with $p13^{suc1}$ wild-type and the single mutant products are consistent with the existence in solution of homogeneous populations of proteins species with nativelike solvent accessibilities (Table 2). Interestingly, a different result was obtained with the double mutant, and a significant deviation from linearity of the Stern−Volmer plot was observed (Figure 8). In the absence of changes of the recovered lifetimes in the presence of 1 M GuHCl, the Stern−Volmer constant can be approximate to diffusional accessibilities. Thus, the results presented are consistent with the assignment of a state with low solvent accessibility to a nativelike protein species and a state with higher solvent accessibility to an intermediate unfolding species. Moreover, the comparison of the K_{SV} quenching constant of the accessible species with the quenching constant of free melatonin in solution revealed that likely the tryptophan residues in the intermediate state are completely exposed to the solvent. For a protein of small dimension as $p13^{suc1}$, this is not a surprising result, and it may suggest that upon substitution of both Pro-90 and Pro-92 either a compact molten globule or a partially unfolded intermediate state is induced.

In the presence of multiple tryptophan residues and complex fluorescence decays of proteins, the relation between the accessible fraction obtained by steady-state measurements and its meaning in terms of actual protein concentration is not straightforward; for this reason a rigorous thermodynamic description of the quenching data cannot be presented. Nonetheless, from our results it seems that relevant information can be obtained on protein accessibility by the combination of fluorescence quenching measurements and denaturant perturbations. In the present study we performed steady-state measurements, and for our purposes a single denaturant concentration was tested. In fact, quencher molecules' diffusion can be measured across an entire titration curve, and changes of the characteristic accessibility can be searched along the full transition of a protein from the native state to the unfolded state. In addition, time-resolved studies can be performed to recover directly diffusional rates, and in favorable cases, experiments can be designed to separate and probe the accessibility of distinct tryptophan residues.

The structural information provided by the present study can be combined with the evidence coming from previous protein engineering studies (*32*) and molecular dynamics simulations (*33*) on $p13^{suc1}$ folding pathways to reach a comprehensive description of the role of Pro-90 and Pro-92 on local domain folding, hinge/arm interactions, and global $p13^{suc1}$ structure. Indeed, from unfolding kinetics studies and computational folding simulation trials it was concluded that (1) $p13^{suc1}$ folds by a nucleation−condensation mechanism, (2) strand β4 forms an integral part of the folding nucleus, and (3) arm-exchange and subunit association is an early event in the folding reaction. Here, on one hand it has been presented that Pro-90 is a determinant by itself in arm exchanging and we propose that one role of residue Pro-90, independent by Pro-92, is crucial in the early dynamics of the folding process and it is related to local β4 arrangements (i.e., folded/extended) which drive the monomer/dimer separation. On the other hand, equilibrium denaturation studies on the double site mutant have indicated the existence of a combined role of residues Pro-90 and Pro-92 on $p13^{suc1}$ structure. It appears that relevant interactions for proper monomer structure and stability are affected. In this form, the insertion of β4 between β3 and β2 is a peculiar feature of the $p13^{suc1}$ β-domain organization. This stable core has been suggested to be relevant in the overall assembling of CKS proteins (*32*, *33*), and it is feasible that hinge destabilization, due to double mutation, allows resolution of some aspects of this process. According to this view, the coordinated molecular role of the two hinge proline residues is effective at late stages of the folding pathway of $p13^{suc1}$, in a process that drives the final refinement of tridimensional organization and stability.

Yet, as previously mentioned, fluorescence-detected denaturation reports processes uniquely related to changes of chain interactions which affect the tryptophan residue environment. For a protein of the size of $p13^{suc1}$ this limitation may be negligible. Nonetheless, it must be noticed that tryptophan-excluded intradomain interactions may elude intrinsic fluorescence detection and conceal a significant part of the process (i.e., $p13^{suc1}$ undergoes an unfolding coupled process). According to this hypothesis, the two-state unfold-

ing transitions recorded with wild type and single mutants could be apparent, with the actual unfolding process that proceeds via destabilization of intradomain interactions followed by cooperative global unfolding. In this respect, double mutation and hinge destabilization would have revealed the "elusive" part of the coupled process.

In conclusion, the results obtained in this study by gel filtration methods on the single mutant proteins are in agreement with a primary role of Pro-90 on p13^{suc1} dimerization by domain swapping. In addition, to our knowledge the potential effects of a double mutation of the β-hinge proline residues on the whole structural organization of CKS were not raised and tested before. In this respect the data obtained with the double mutant P90/P92V have provided novel information on the role and the significance of proline's repeat motifs in proteins and, in particular, in the stabilization of crucial β-strands of CKS.

In the end, although the understanding of the actual molecular role of each proline residue may require further investigation supported by specific experimental designs at atomic resolution (i.e., X-ray and NMR), the results obtained revealed significant information on the p13^{suc1} structure and oligomerization mechanism.

ACKNOWLEDGMENT

We thank Drs. G. Gallinella, A. R. Musa, and C. Menna for their valuable guidance and help in preparing the SUC1 constructs. We also thank Prof. G. P. Bagnara and Dr. R. Tonelli for DNA sequencing and Dr. Paola Turina for helpful discussion and careful reading of the manuscript. Gel protein documentation and analytical size-exclusion chromatography were carried out using the facilities of the Interdepartmental Center for Biotechnology Research of the University of Bologna.

REFERENCES

1. Morgan, O. M. (1995) *Nature 374*, 131−134.
2. Sherr, C. J., and Roberts, J. M. (1999) *Genes Dev. 13*, 1501−1512.
3. Booher, R., Holman, P. S., and Fattaey, A. (1997) *J. Biol. Chem. 272*, 22300−22306.
4. Palmer, A., Gavin, A.-C., and Nebreda, R. (1998) *EMBO J. 17*, 5037−5047.
5. Wells, N. J., Watanabe, N., Tokosumi, T., Jiang, W., Verdecia, M. A., and Hunter, H. (1999) *J. Cell Sci. 112*, 3361−3371.
6. De Bondt, H. L., Rosenblatt, J., Jancarik, J., Jones, H. D., Morgan, M. O., and Kim, S.-H. (1993) *Nature 363*, 595−602.
7. Brown, N. R., Noble, M. E. M., Endicott, J. A., Garman, E. F., Wakatsuki, S., Mitchell, E., Rasmussen, B., Hunt, T., and Johnson, L. N. (1995) *Structure 3*, 1235−1247.
8. Jeffrey, P. D., Russo, A. A., Polyak, K., Gibbs, E., Hurwitz, J., and Pavletich, N. P. (1995) *Nature 376*, 313−320.
9. Russo, A. A., Jeffrey, P. D., and Pavletich, N. P. (1996) *Nat. Struct. Biol. 3*, 696−700.
10. Russo, A. A., Jeffrey, P. D., Patten, A., Massague, J., and Pavletich, N. P. (1996) *Nature 382*, 325−331.
11. Pines, J. (1996) *Curr. Biol. 6*, 1399−1402.
12. Hadwiger, J. A., Wittenberg, C., Mendenhall, M. D., and Reed, S. I. (1989) *Mol. Cell. Biol. 9*, 2034−2041.
13. Hayles, J., Beach, D., Durkacz, B., and Nurse P. (1986) *Mol. Gen. Genet. 202*, 291−293.
14. John, P. C. L., Zhang, K., and Dong, C. (1993) in *Molecular and Cell Biology of the Plant Cell Cycle* (Ormrod, J. C., and Francis, D., Eds.) pp 9−34, Kluwer, Norwell, MA.
15. Brizuela, L., Draetta, G., and Beach, D. (1987) *EMBO J. 6*, 3507−3514.
16. Dunphy, W. G., and Newport, J. (1989) *Cell 58*, 181−191.
17. Dunphy, W. G., Brizuela, L., Beach, D., and Newport, J. W. (1988) *Cell 54*, 423−431.
18. Gavin, A. C., Vassalli, J. D., Cavadore, J. C., and Schorderet-Slatkine, S. (1992) *Mol. Reprod. Dev. 33*, 287−296.
19. Patra, D., Wang, S. X., Kumagai, A., and Dunphy, W. G. (1999) *J. Biol. Chem. 274*, 36839−36842.
20. Patra, D., and Dunphy, W. G. (1998) *Genes Dev. 12*, 2549−2559.
21. Sudakin, V., Shteiberg, M., Ganoth, D., Hershko, J., and Hershko, A. (1997) *J. Biol. Chem. 272*, 18051−18059.
22. Shteiberg, M., and Hershko, A. (1999) *Biochem. Biophys. Res. Commun. 257*, 12−18.
23. Bourne, Y., Arva, A. S., Bemstein, S. L., Watson, M. H., Reed, S. I., Endicott, J. E., Noble, M. E., Johnson, L. N., and Tainer, J. A. (1995) *Proc. Natl. Acad. Sci. U.S.A. 92*, 10232−10236.
24. Endicott, J. A., Noble, M. E., Garman, E. F., Brown, N., Rasmussen, B., Nurse, P., and Johnson, L. N. (1995) *EMBO J. 14*, 1004−1014.
25. Khazanovich, N., Batema, K. S., Chernaia, M., Michalak, M., and James, M. N. G. (1996) *Structure 4*, 299−309.
26. Parge, H. E., Arvai, A. S., Murtari, D. J., Reed S. I., and Tainer, J. A. (1993) *Science 262*, 387−394.
27. Bourne, Y., Watson, M. H., Hickey, M. J., Holmes, W., Rocque, W., Reed, S. I., and Tainer, J. A. (1996) *Cell 84*, 863−874.
28. Bergdoll, M., Remy, M.-H., Cagnon, C., Masson, J.-M., and Dumas, P. (1997) *Structure 5*, 391−401.
29. Bennett, M. J., Schlunegger, M. P., and Eisenberg, D. (1995) *Protein Sci. 4*, 2455−2468.
30. Watson, M. H., Bourne, Y., Arvai, A. S., Hickey, J. M., Santiago, A., Bernstein, S. L., Tainer, J. A., and Reed, S. I. (1996) *J. Mol. Biol. 261*, 646−657.
31. Rousseau, F., Schymkowitz, J. W. H., Sánchez del Pino, M., and Itzhaki, L. S. (1998) *J. Mol. Biol. 284*, 503−519.
32. Schymkowitz, J. W. H., Rousseau, F., Irvine, L. R., and Itzhaki, L. S. (2000) *Structure 8*, 89−100.
33. Alonso, D. O. V., Alm, E., and Daggett, V. (2000) *Structure 8*, 101−110.
34. Birck, C., Vachette, P., Welch, M., Swarén, P., and Samama, J. P. (1996) *Biochemistry 35*, 5577−5585.
35. Neyroz, P., Menna, C., Polverini, E., and Masotti, L. (1996) *J. Biol. Chem. 271*, 27249−27258.
36. Lowry, O. H., Rosebrough, N. J., Farr, A. L., and Randall, R. J. (1951) *J. Biol. Chem. 193*, 265−275.
37. Bradford, M. (1976) *Anal. Biochem. 72*, 248−254.
38. Laemmli, U. K. (1970) *Nature 227*, 680−685.
39. Fisher, L., and Guo, K. P. (1997) *BioTechniques 23*, 570−574.
40. Creighton, T. E. (1993) in *Proteins*, 2nd ed., W. H. Freeman and Co., New York.
41. Lehrer, S. S. (1971) *Biochemistry 10*, 3254−3263.
42. Lakowicz, J. R. (1983) *Principles of Fluorescence Spectroscopy*, Plenum Press, New York.
43. Laws, W. R., and Contino, P. B. (1992) *Methods Enzymol. 210*, 448−463.
44. Grinvald, A., and Steinberg, I. Z. (1974) *Anal. Biochem. 59*, 583−598.
45. Beechem, J. M., Ameloot, M., and Brand, L. (1985) *Anal. Instrum. 14*, 379−402.
46. Bevington, P. R. (1969) in *Data Reduction and Error Analysis for the Physical Science*, McGraw-Hill Inc., New York.
47. Beechem, J. M., Gratton, E., Ameloot, M., Knutson, J. R., and Brand, L. (1991) in *Topics in Fluorescence Spectroscopy: Principles II* (Lakowicz, J. R., Ed.) pp 241−305, Plenum Press, New York.
48. Pace, C. N. (1986) *Methods Enzymol. 131*, 266−280.

49. Eftink, M. R. (1994) *Biophys. J. 66*, 482−501.
50. Knutson, J. R., Walbridge, D. G., and Brand, L. (1982) *Biochemistry 21*, 4671−4679.
51. Neyroz, P., Desdouits, F., Benfenati, F., Knutson, J. R., Greengard, P., and Girault, J.-A. (1993) *J. Biol. Chem. 268*, 24022−24031.
52. Hogue, C. W., Doublie, S., Wong, J. T., Carter, C. W., Jr., and Szabo, A. G. (1996) *J. Mol. Biol. 260*, 446−466.
53. Lam, W. C., Seifert, J. M., Amberger, F., Graf, C., Auer, M., and Millar, D. P. (1998) *Biochemistry 37*, 1800−1809.
54. Polverini, E., Casadio, R., Neyroz, P., and Masotti L. (1998) *Arch. Biochem. Biophys. 349*, 225−235.
55. Ewbank, J. J., Creighton, T. E., Hayer Hartl, M. K., and Ulrich Hartl, F. (1995) *Nat. Struct. Biol. 2*, 10−11.

BI002812D